

1 ***Porphyromonas gingivalis* outer membrane vesicles in cerebral ventricles activate**
2 **microglia in mice**

3

4

5 Kayo Yoshida¹, Kaya Yoshida^{2*}, Mariko Seyama¹, Yuka Hiroshima³, Mana Mekata¹, Natsumi
6 Fujiwara¹, Yasusei Kudo⁴, Kazumi Ozaki¹

7

8 Departments of ¹Oral Healthcare Promotion, ²Oral Healthcare Education, ³Oral Microbiology, ⁴Oral
9 Bioscience, Institute of Biomedical Sciences, Tokushima University Graduate School, 3-18-15

10 Kuramoto, Tokushima 770-8504, Japan

11

12 *Address correspondence to:

13 Kaya Yoshida, DDS, PhD

14 3-18-15, Kuramoto, Tokushima 770-8504, Japan

15 TEL: 81-88-633-7898, FAX: 81-88-633-7898

16 E-mail:kaya@tokushima-u.ac.jp

17

18

19 **Email address of co-author**

20 Kayo Yoshida; c302141001@tokushima-u.ac.jp

21 Mariko Seyama; seyama.mariko@tokushima-u.ac.jp

22 Yuka Hiroshima; yuka.hiroshima@tokushima-u.ac.jp

23 Mana Mekata; c302231002@tokushima-u.ac.jp

24 Natsumi Fujiwara; nfujiwara@tokushima-u.ac.jp

25 Yasusei Kudo; yasusei@tokushima-u.ac.jp

26 Kazumi Ozaki; ozaki@tokushima-u.ac.jp

27

28 **Funding**

29 This study was supported by Grant-in-Aid for Scientific Research from the Ministry of Education,
30 Science, Sports, and Culture of Japan (20K21714, Kaya Yoshida; 20K23030, MS)

31

32 **Conflict of interest disclosure**

33 The authors declare that they have no known competing financial interests or personal relationships

34 that could have appeared to influence the work reported in this paper.

35

36 **Ethics approval statement**

37 Mice were housed under specific pathogen-free conditions according to the Fundamental Guidelines

38 for Proper Conduct of Animal Experiments and Related Activities in Academic Research Institutions

39 (the Ministry of Education, Culture, Sports, Science and Technology, Japan, 2006). All animal

40 experiments were approved by the Ethics Committee of Animal Care and Experimentation of

41 Tokushima University (approval number: T29-31).

42

43 **Abbreviations**

44 *Pg*, *Porphyromonas gingivalis*; AD, Alzheimer's disease; OMV, outer membrane vesicle; LPS,

45 lipopolysaccharide; TNF- α , tumor necrosis factor-alpha; IL-6, interleukin-6; ATCC, American Type

46 Culture Collection; CSF, cerebrospinal fluid; BBB, blood brain barrier; BCSFB, blood-cerebrospinal
47 fluid barrier
48
49 Running title
50 *P. gingivalis* OMVs induce neuroinflammation
51

52 **Abstract**

53 **Objective:** *Porphyromonas gingivalis* (*Pg*) is thought to be involved in the progression of Alzheimer's
54 disease (AD). Whether *Pg* or its contents can reach the brain and directly affect neuropathology is,
55 however, unknown. Here, we investigated whether outer membrane vesicles (OMVs) of *Pg* translocate
56 to the brain and induce the pathogenic features of AD.

57 **Material and Methods:** *Pg* OMVs were injected into the abdominal cavity of mice for 12 weeks. *Pg*
58 OMV translocation to the brain was detected by immunohistochemistry using an anti-gingipain
59 antibody. Tau protein and microglial activation in the mouse brain were examined by western blotting
60 and immunohistochemistry. The effect of gingipains on inflammation was assessed by real-time
61 polymerase chain reaction using human microglial HMC3 cells.

62 **Results:** Gingipains were detected in the region around cerebral ventricles, choroid plexus, and
63 ventricular ependymal cells in *Pg* OMV-administered mice. Tau and phosphorylated Tau protein
64 increased and microglia were activated. *Pg* OMVs also increased the gene expression of
65 proinflammatory cytokines in HMC3 cells in a gingipain-dependent manner.

66 **Conclusion:** *Pg* OMVs, including gingipains, can reach the cerebral ventricle and induce
67 neuroinflammation by activating microglia. *Pg* OMVs may provide a better understanding of the
68 implications of periodontal diseases in neurodegenerative conditions such as AD.

69

70

71 **Keywords** *Porphyromonas gingivalis*, outer membrane vesicle, gingipain, neuroinflammation,

72 microglia, cerebral ventricle

73

74

75 1. Introduction

76 *Porphyromonas gingivalis* (*Pg*) is a gram-negative bacterium known to be a key pathogen in periodontal
77 diseases (Genco & Borgnakke, 2013). *Pg* expresses various types of virulence factors, including the
78 gingipain family proteins, arginine-specific gingipains (RgpA and RgpB) and lysine-specific gingipain
79 (Kgp), that contribute to the progression of periodontal diseases by destroying periodontal tissues
80 (Gabarrini, Grasso, van Winkelhoff, & van Dijk, 2020; O'Brien-Simpson, Pathirana, Walker, &
81 Reynolds, 2009). Periodontal diseases have been implicated in the pathogenesis of Alzheimer's disease
82 (AD) (Ingar Olsen & Singhrao, 2020). Gingipains have been detected in the brains of patients with AD,
83 and small-molecule inhibitors of gingipains are known to rescue the neurodegeneration in the *Pg*-
84 infected brain (Dominy et al., 2019). *Pg* lipopolysaccharide (LPS) has also been detected in the brains
85 of AD patients (Poole, Singhrao, Kesavalu, Curtis, & Crean, 2013). In mouse models, *Pg* infection can
86 exacerbate the features of AD with an increase in *Pg* LPS in the brain (Ishida et al., 2017).

87 AD is a neurodegenerative disease characterized by chronic inflammation of the brain (Akiyama et al.,
88 2000). The microglia, which are immune effective cells in the brain, are activated by amyloid deposits
89 and secrete a variety of pro-inflammatory cytokines, which contribute to the progression of AD
90 (Mandrekar-Colucci & Landreth, 2010). *Pg* has been proposed to induce neuroinflammation by
91 activating microglia in AD (I. Olsen, 2021). *Pg* LPS-induced periodontitis impairs recognition in rats
92 through neuroinflammation by activating microglia (Yoshiyama et al., 2007). Gingipains have also been
93 reported to be responsible for the migration and activation of microglia by *Pg* (Liu et al., 2017; Nonaka
94 & Nakanishi, 2020). These observations suggest that *Pg* infection in the oral cavity may affect the
95 distant brain tissue and increase the risk of AD. However, it is still debatable whether *Pg* or its contents
96 such as LPS and gingipains can cross anatomical structures such as the blood-brain barrier (BBB),
97 which inhibits the penetration of small molecules from the blood to the central nervous system and
98 prevents neuropathology in the brain.

99 Similar to other gram-negative bacteria, *Pg* releases abundant outer membrane vesicles (OMVs) during
100 its growth in various environments, including lipid culture and biofilms. Given their small size (50-70

101 nm in diameter) and adhesive and proteolytic properties, OMVs are thought to fuse with host cells and
102 deliver their contents directly into the cytosol. Further, OMVs can spread more readily in the tissue than
103 in bacterial cells (Kuehn & Kesty, 2005). *Pg* OMVs contain most of *Pg* virulence factors such as
104 gingipains and LPS and are internalised into the host cell, which results in modulation of various
105 responses. For instance, gingipains present on the surface of *Pg* OMVs increased vascular permeability
106 both *in vitro* and *in vivo* via proteolytic cleavage of endothelial cell-cell adhesion (Farrugia, Stafford,
107 & Murdoch, 2020). Recently, we also observed that *Pg* OMVs injected into the abdominal cavity could
108 reach the liver and inhibit hepatic glycogenesis, resulting in high blood glucose levels in mice (Seyama
109 et al., 2020). These observations prompted us to hypothesize that *Pg* OMVs could be an alternative
110 mechanism by which *Pg* transmits virulence factors to distant organs in the body and eventually induce
111 extraoral diseases.

112 In this study, we examined whether *Pg* OMVs translocate to the brain and increase the risk of AD. We
113 isolated OMVs from the culture medium of *Pg* and intraperitoneally injected them into mice. The
114 translocation of *Pg* OMVs to the brain tissue was detected by immunohistochemistry using an anti-
115 gingipain antibody. We also examined the effect of *Pg* OMVs on tau protein expression and microglial
116 activation, which are pathogenic features of AD, using mouse or human microglial HMC3 cells.

117

118 **2. Materials and Methods**

119 **2.1. Bacterial culture and isolation of *Pg* OMVs**

120 *Porphyromonas gingivalis* (*Pg*) ATCC 33277 was cultured in brain heart infusion medium (BD
121 Bioscience, Franklin Lakes, NJ, USA) containing 0.5% yeast extract (BD Bioscience), 10 µg/mL hemin
122 (Wako Chemicals, Osaka, Japan), and 1 µg/mL 2-methyl-1, 4-naphthoquinone (Tokyo Kasei, Tokyo,
123 Japan) in an anaerobic jar at 37°C. The gingipain mutant of *Pg* ATCC 33277 (KDP136) was kindly
124 provided by Dr. Koji Nakayama (Nagasaki University) and cultured in the aforementioned medium
125 containing 25 µg/mL chloramphenicol, 10 µg/mL erythromycin, and 1 µg/mL tetracycline.

126 *Pg* OMVs were isolated using an established protocol (Eguchi et al., 2018; Ono et al., 2018) as described
127 in our previous report (Seyama et al., 2020). Briefly, the culture medium of *Pg* was centrifuged at 2800
128 ×g for 15 min at 4 °C. The supernatant was filtered with a 0.2 µm syringe filter and then concentrated
129 using Ultra-15 Centrifugal Filter Device for nominal molecular weight limit (NMWL) 100,000
130 (Amicon, Merck, Tokyo, Japan). The concentrate was mixed with Total Exosome Isolation Reagent
131 (Thermo Fisher Scientific, Tokyo, Japan) and incubated overnight at 4°C. The sample was centrifuged
132 at 10,000 ×g for 60 min at 4°C, and the *Pg* OMV fraction was obtained by eluting the pellet in 100 µL
133 phosphate-buffered saline PBS (-).

134

135 **2.2. Animals**

136 BALB/cAJc1 mice (female, 40 weeks old) were purchased from Japan CLEA (Tokyo, Japan) and fed
137 a high-fat diet (Quick Fat, 15.3% fat, 424.5 kcal/100 g; Japan CLEA). Mice were housed under specific
138 pathogen-free conditions according to the Fundamental Guidelines for Proper Conduct of Animal
139 Experiments and Related Activities in Academic Research Institutions (the Ministry of Education,
140 Culture, Sports, Science and Technology, Japan, 2006). All animal experiments were approved by the
141 Ethics Committee of Animal Care and Experimentation of Tokushima University (approval number:
142 T29-31).

143

144 **2.3. Immunohistochemistry**

145 *Pg* OMVs (5 µg of total protein) or PBS was intraperitoneally injected into mice for 12 weeks at a 3-
146 day interval. After the indicated time periods, mouse brain tissues were excised and fixed in 4%
147 paraformaldehyde-containing phosphate buffer solution (Nacalai Tesque) for 48 h at 4°C. The tissues
148 were then embedded in paraffin wax and sectioned at 4 µm thickness. Paraffin was removed from
149 sections using xylene and ethanol. The sections were heated in a 0.1 M buffer to retrieve antigens,
150 followed by incubation in 0.3% hydrogen peroxide (H₂O₂) in methanol for 30 min. After blocking with
151 4% bovine serum albumin (BSA) in PBS for 60 min, the sections were incubated with anti-Kgp/Rgp

152 antibody (1:800), Iba1 (1:500, GTX100042, Gene Tex), or normal rabbit IgG for 16 h at 4°C. The rabbit
153 polyclonal antibody against Kgp/Rgp was kindly provided by Dr. Tomoko Kadowaki of Nagasaki
154 University (Takii, Kadowaki, Baba, Tsukuba, & Yamamoto, 2005). Immunoreactive sites were
155 identified using the SignalStain Boost Detection reagent (Cell Signaling Technology) and observed
156 using a BZ-X800 microscope (Keyence).

157

158 ***2.4. Sodium dodecyl sulphate polyacrylamide gel electrophoresis (SDS-PAGE) and western blotting*** 159 ***analysis***

160 After 12 weeks of *Pg* OMV administration, the brains were excised and homogenized in a lysate buffer
161 (1 mM dithiothreitol [DTT], 0.2 mM phenylmethylsulfonyl fluoride [PMSF], 1 µg/mL leupeptin, 4
162 µg/mL aprotinin, and 50 mM sodium fluoride [NaF]). Ten micrograms of each sample were separated
163 by SDS-PAGE and transferred to polyvinylidene fluoride membranes (Millipore, Billerica, MA, USA).
164 The membranes were incubated for 1 h at ambient temperature in 5% non-fat skim milk in Tris-buffered
165 saline (TBS) containing 0.05% Tween-20 (TBS-Tween) and then incubated overnight at 4°C in a
166 blocking solution containing specific antibodies. The primary antibodies used were phospho-Tau
167 (Ser202, Thr205) (AT8) (1:1000, MN1020, Thermo Fisher Scientific), Tau (D1M9X) (1:1000, #46687,
168 Cell Signaling Technology), and glyceraldehyde 3-phosphate dehydrogenase (GAPDH; 1:1000, 60008-
169 1, Proteintech). After washing with PBS-Tween, the membranes were incubated for 1 h at room
170 temperature in a blocking solution containing horseradish peroxidase-conjugated secondary antibodies
171 (dilution, 1:5000). The membranes were then washed, and the signals were detected using a western
172 blot chemiluminescence horseradish peroxidase (HRP) substrate (Takara) according to the
173 manufacturer's instructions.

174 The images of the bands obtained by western blotting were scanned and quantified using ImageJ version
175 1.47. Densitometry of Tau and phospho-Tau was normalized to that of GAPDH. The ratios of
176 Tau/GAPDH and phospho-Tau/GAPDH are shown.

177

178 **2.5. Cell culture**

179 Human embryonic microglial clone HMC3 cells (ATCC: CRL-3304) were obtained from the American
180 Type Culture Collection (ATCC; Manassas, VA, USA). HMC3 cells were plated in plastic dishes at a
181 density of 10×10^4 cells/ mL in Dulbecco's modified Eagle's medium (DMEM) supplemented with
182 10% fetal bovine serum (FBS) at 37°C under a humidified atmosphere of 5% CO₂.

183

184 **2.6. Real-time PCR**

185 After reaching 70-80% confluence, HMC3 cells were treated with or without Pg OMVs at a
186 concentration of 500 ng/mL for 3 h. Total RNA was isolated from HMC3 cells using ISOGEN (Nippon
187 Gene), according to the manufacturer's protocol. The cDNA was synthesised using the Prime Script™
188 RT Reagent Kit (Takara Bio, Kyoto, Japan). Real-time PCR was performed using the 7300 Real-Time
189 PCR system (Applied Biosystems, Carlsbad, CA, USA) with SYBR Premix Ex Taq™ (Takara Bio).
190 The following primer sequences were used: human GAPDH (NM_002046.7) forward, 5'-
191 GCACCGTCAAGGCTGAGAAC-3' and reverse, 5'-TGGTGAAGACGCCAGTGGA-3'; human
192 tumor necrosis factor-alpha (TNF- α , NM_000594) forward, 5'-
193 GACAAGCCTGTAGCCCATGTTGTA-3' and reverse, 5'-CAGCCTTGGCCCTTGAAGA-3'; human
194 interleukin-6 (IL-6; NM_000600.5) forward, 5'-AAGCCAGAGCTGTGCAGATGAGTA-3' and
195 reverse, 5'-TGTCCTGCAGCCACTGGTTC-3'.

196

197 **2.7. Statistical analysis**

198 Statistical analyses were performed using the Statcel2 software. The normal distribution of the data
199 was first examined using the chi-square test. Variables that had a normal distribution were analyzed
200 using the Student's *t*-test.

201

202 **3. Results**

203 **3.1. Gingipains were detected around the cerebral ventricle in Pg OMV-administered mice**

204 To examine the effects of *Pg* OMVs on neuropathology, *Pg* OMVs or PBS was administered into the
205 abdominal cavities of mice for 12 weeks and the brain tissues were excised after the treatment. We first
206 confirmed whether intraperitoneally injected-*Pg* OMVs could reach the brains of mice. As we have
207 previously shown that *Pg* OMVs contain the gingipain variants Kgp and Rgp (Seyama et al., 2020), the
208 translocation of *Pg* OMVs to the brain was assessed by immunohistochemistry using antibodies against
209 Kgp/Rgp.

210 In the brains of PBS-treated mice, no gingipain-specific staining was observed in any region (Fig. 1a,
211 b). In the brains of *Pg* OMV-administered mice, gingipains were detected in the extracellular spaces in
212 regions near cerebral ventricles (Fig. 1c-e). The positive reaction of gingipains was visualized as a dot-
213 shaped deposition in the extracellular space (Fig. 1e, open arrowheads). Staining with normal rabbit
214 IgG instead of anti-Rgp/Kgp antibody failed to detect a positive signal (Fig. 1f), indicating the
215 gingipain-specific staining. These findings suggest that *Pg* OMVs injected into the abdominal cavity
216 were translocated with their cargo gingipains into the mouse brain.

217

218 ***3.2. Gingipains were detected in the choroid plexus and ventricular ependymal cells of *Pg* OMV-*** 219 ***administered mice***

220 Interestingly, gingipains were detected only in the region near the cerebral ventricle, but not in the
221 cerebral cortex, of *Pg* OMV-administered mice. This observation prompted us to further dissect the
222 pathway of *Pg* OMVs to the brain from the bloodstream. As small molecules in the systemic blood are
223 known to leak from the choroid plexus to the cerebrospinal fluid (CSF) (Gherzi-Egea & Strazielle,
224 2001), we investigated the presence of gingipains in the choroid plexus and ependymal cells
225 surrounding the cerebral ventricle. Immunohistochemistry results showed no positive staining of
226 gingipains in the choroid plexus of PBS-treated mice (Fig. 2a, 2b). In *Pg* OMV-administered mice, the
227 positive signal of gingipains was observed in the perinuclear region of the choroid plexus epithelial
228 cells (Fig. 2d, 2e, closed arrowheads) and blood vessels within the choroid plexus (Fig. 2e, arrows).
229 Consistent with the results in Figure 1, gingipains were also detected in the extracellular spaces of the

230 brain around the ventricle (Fig. 2e, open arrowheads). The brain sections from *Pg* OMV-treated mice
231 showed negative staining when probed with normal rabbit IgG (Fig. 2f).

232 We next determined the presence of gingipains in ependymal cells, the ciliated cuboidal cells without
233 basal lamina that line the surface of the cerebral ventricle. Similar to the choroid plexus epithelial cells,
234 gingipains were localised in the perinuclear regions of ependymal cells from *Pg* OMV-administered
235 mice (Fig. 2d, 2g, closed arrowheads) but not in those from PBS-treated mice (Fig. 2c). In extracellular
236 spaces near ependymal cells, gingipains were visualised as dot-shaped deposits (Fig. 2g, open
237 arrowheads). These positive reactions with gingipains were not observed in the brain probed with
238 normal rabbit IgG (Fig. 2h). Altogether, these results suggest that the choroid plexus and ependymal
239 cells in cerebral ventricles are likely to be the pathways of *Pg* OMVs to the brain.

240

241 ***3.3. Tau and phosphorylated-Tau protein levels increased in the brains of *Pg* OMV-administered*** 242 ***mice***

243 Tau is a microtubule-associated protein that regulates the microtubule assembly and stabilises neurons.
244 As Tau aggregation and phosphorylation could be the key events in the development of AD (Perea,
245 Bolós, & Avila, 2020), we examined whether *Pg* OMV administration modulates the status of Tau
246 protein in the brain of mice. Brain tissues were excised from the mice injected with *Pg* OMVs or PBS
247 for 12 weeks and prepared for western blotting. As shown in Figure 3A, the expression levels of Tau
248 and phosphorylated-Tau (p-Tau) increased in the brains of *Pg* OMV-administered mice (Fig. 3A). The
249 results of western blotting for total Tau and phosphorylated Tau proteins were quantified using ImageJ
250 software and compared between the groups. The Tau /GAPDH ratio was significantly higher in the
251 brains of *Pg* OMV-treated mice (2.426 ± 0.155 , $p = 0.002$) than in the brains of PBS-treated mice (1.000
252 ± 0.434). The administration of *Pg* OMVs also increased the p-Tau /GAPDH ratio (1.881 ± 0.157 , $p =$
253 0.013) compared to that in the PBS-treated group (1.000 ± 0.406).

254

255 The ratios of Tau/GAPDH and p-Tau/GAPDH in each group are presented for mice treated with PBS

256 (n = 4) or *Pg* OMV (n = 4) and analysed by the Student's *t*-test. Values are shown as the fold change in
257 expression levels in the PBS group. * $p < 0.05$, ** $p < 0.01$ as compared with mice treated with PBS.
258 Both total and phosphorylated Tau protein levels were significantly higher in the brains of *Pg* OMV-
259 administered mice than in the brains of PBS-treated mice (Fig. 3B).

260

261 ***3.4. Microglia were activated in the brains of *Pg* OMV-administered mice***

262 Microglia are activated under pathological conditions and play a complex role in AD progression
263 (Mandrekar-Colucci & Landreth, 2010). Therefore, we examined whether *Pg* OMVs affected
264 microglial activation. The activated microglia showed morphological changes characterized with an
265 amoeboid cell body with short processes (Diz-Chaves, Pernía, Carrero, & Garcia-Segura, 2012).
266 Therefore, we visualized microglia by staining with an antibody specific for the microglial marker Iba1
267 and observed their morphology in the brains of both groups of mice.

268 In PBS-treated mice, several Iba1-immunoreactive cells were observed near the cerebral ventricle (Fig.
269 4A, a, b). Most of these cells had a small cell body with longer cell processes (Fig. 4A, c). Iba1-
270 immunoreactive cells were also detected around the cerebral ventricle in *Pg* OMV-administered mice
271 (Fig. 4A, d, e). In these mice, the proportion of cells with amoeboid cell bodies was higher than that
272 observed in control mice (Fig. 4A, f). We also examined *Pg* OMV effects on microglia in the
273 hippocampus. Similar to the observation around the cerebral ventricle, *Pg* OMV administration
274 increased the number of microglia with amoeboid cell bodies and the intensity of Iba1 staining (Fig.
275 4B, d-f) in the hippocampus; these types of cells were not observed in PBS-treated mice (Fig. 4B, a-c).
276 These results suggest that *Pg* OMV administration induced the activation of microglia in the mouse
277 brain.

278

279 ***3.5. *Pg* OMVs increased the expression of proinflammatory cytokine genes in a gingipain-dependent*** 280 ***manner in HMC3 cells***

281 Although our histological experiments (Figs 1, 2, and 4) suggested that *Pg* OMVs, including gingipains,
282 could translocate to the brain where microglia are activated, whether gingipains are involved in the
283 activation of microglia is yet unknown. As activated microglia produce cytokines to promote
284 neuroinflammation and exacerbate neuropathology in AD (W. Y. Wang, Tan, Yu, & Tan, 2015), we
285 examined the effects of *Pg* OMVs on the expression of pro-inflammatory cytokine genes in human
286 microglial HMC3 cells.

287 OMVs were isolated from the culture medium of the KDP136 strain of *Pg*, which is Kgp/Rgp double-
288 deficient. We previously confirmed that OMVs of the KDP136 strain lack both Kgp and Rgp gingipains
289 (Seyama et al., 2020). HMC3 cells were incubated with OMVs derived from the wild-type *Pg* (*Pg*
290 OMVs [WT]) or KDP136 (*Pg* OMVs [K136]) strain for 3 h, and the expression of genes was analyzed
291 by real-time PCR. As shown in Figure 5, treatment with *Pg* OMVs (WT) significantly increased the
292 expression of inflammatory genes such as *IL-6*, *TNF- α* , *IL-8*, and *IL-1 β* . In contrast, *Pg* OMVs (K136)
293 failed to upregulate the expression of these genes (Fig. 5). These results suggest that gingipains on *Pg*
294 OMVs are responsible for the induction of pro-inflammatory cytokine expression in HMC3 cells.

295

296 **4. Discussion**

297 The presence of *Pg* OMVs in body fluids such as blood, saliva, and GCF of patients with periodontal
298 diseases has not been investigated to date, whereas genomic DNA qPCR revealed that the relative levels
299 of salivary *Pg* OMVs increased in the periodontitis group when compared to that in the healthy group
300 (P. Han, Bartold, Salomon, & Ivanovski, 2021). Therefore, we injected *Pg* OMVs (5 mg of protein)
301 into mice, which affected glucose metabolism in a mouse model as reported in our previous study
302 (Seyama et al., 2020).

303 *Pg* OMV has been considered as an alternative factor that causes neurodegenerative diseases in the
304 brain, such as AD, because of its small size and rich content of virulence factors (Nara, Sindelar, Penn,
305 Potempa, & Griffin, 2021; Singhrao & Olsen, 2018). However, there is no direct evidence that *Pg* OMV
306 can access the brain and is implicated in AD pathogenesis. In this study, we first examined whether *Pg*

307 OMVs translocate to the mouse brain. As bacterial OMVs lack known unique biological markers, we
308 attempted to track *Pg* OMVs by detecting their cargo protein gingipains. In cultured cells, but not in
309 mouse models, *Pg* virulence factors such as gingipains and fimbriae are often used to detect the
310 localization of *Pg* OMVs. For instance, Furuta et al. observed that *Pg* OMVs probed with antibodies
311 against native fimbriae could invade HeLa and human gingival epithelial cells via a lipid-raft endocytic
312 pathway (Furuta et al., 2009). Cy5-labelled *Pg* OMVs overlapped with immunostaining signals with
313 the antibody against gingipain, indicating that gingipain could be used to detect the localisation of *Pg*
314 OMVs. Consistent with these reports, positive staining for gingipain was observed in the brains of *Pg*
315 OMV-administered mice (Figs 1 and 2), suggesting that *Pg* OMVs injected into the abdominal cavity
316 may be translocated to the brain via the bloodstream in the body; however, the presence of gingipains
317 or *Pg* OMVs in the blood serum was not determined.

318 The mechanisms underlying the translocation of *Pg* OMVs to the brain remain unclear. Both *in vitro*
319 and *in vivo* experiments have revealed that *Pg* OMVs increase vascular permeability by disrupting tight
320 junction proteins of endothelial cells in the systemic and cerebral vasculature in a gingipain-dependent
321 manner (Farrugia, Stafford, & Murdoch, 2020; Farrugia, Stafford, Potempa, et al., 2020; Nonaka,
322 Kadowaki, & Nakanishi, 2022; Pritchard et al., 2022). These properties are thought to enable *Pg* OMVs
323 to pass through the BBB in the CNS; however, there have been no reports of direct visualisation of *Pg*
324 OMVs in the brain. Recently, OMVs from another periodontal bacterium, *Aggregatibacter*
325 *actinomycetemcomitans* (*Aa*), were tracked to the brain using the clearing technique and two-
326 dimensional light sheet fluorescence microscopy analysis (E. C. Han et al., 2019). The lipophilic tracer
327 DiD-labeled *Aa* OMVs were detected in the cortical extracellular space around the microvessels 24 h
328 after intracardiac injection. These *Aa* OMVs were also co-localized with RNAs inside OMVs in the
329 cortex region, indicating that *Aa* OMVs can pass through the BBB and are present in the cortex of
330 mouse brains. However, in contrast to *Aa* OMVs, we detected positive staining of gingipains only
331 in/near the region of the lateral ventricle, but not in other parts of the brain such as the cortex (Figs 1
332 and 2).

333 Although the BBB has been mainly investigated as the pathway by which bacterial OMVs enter the
334 brain, small molecules in the systemic blood are known to leak from the choroid plexus into the CSF
335 (Gherzi-Egea & Strazielle, 2001). This barrier between the choroid plexus and CSF is called the blood-
336 cerebrospinal fluid barrier (BCSFB). The choroid plexus consists of blood vessels embedded in the
337 stroma that are enclosed by epithelial cells. As the vascular endothelial cells herein are fenestrated and
338 the capillaries are thin-walled, unlike those in the BBB, solutes in the blood can easily leak into the
339 stroma of the choroid plexus (Johanson et al., 2017). The epithelium enclosed within the choroid plexus
340 has low electrical resistance and is much more permeable than the BBB (Nguyen Hoang, 2019).
341 Therefore, solutes in the stroma diffuse into the CSF. The ependymal cells lining the ventricle have
342 incomplete tight junctions, which transport the solutes in the CSF to the extracellular spaces of the brain
343 (Lippoldt et al., 2000; Oliver et al., 2013). These observations indicate that BCSFB has more permeable
344 features than BBB; therefore, it was recently proposed as an alternative route for the uptake of *Pg* OMVs
345 by the brain (Nara et al., 2021).

346 Indeed, we detected gingipains in the choroid plexus and ventricular ependymal cells, in addition to the
347 extracellular spaces around the ventricle (Figs 1 and 2), suggesting that *Pg* OMVs possibly leaked from
348 the blood to the brain via BCSFB. Notably, the gingipain-detected region was located around the
349 inferior horn of the lateral ventricle. This part of the lateral ventricle contains abundant choroid plexus
350 and is located downward following the outer surface of the hippocampus. These anatomical structures
351 seem to allow *Pg* OMVs to reach the lateral ventricle, suggestive of its involvement in the pathogenesis
352 of AD through its effect on the hippocampus. The report showing that *Pg* DNA was detected in the CSF
353 of patients diagnosed with probable AD seems to be consistent with this concept (Dominy et al., 2019).
354 Further investigations are warranted to track the pathway by which *Pg* OMVs enter the brain using, for
355 example, an *in vivo* imaging system.

356 In this study, we also found that the microglia around the lateral ventricle changed their morphology to
357 cells with amoeboid cell bodies in *Pg* OMV-injected mice (Fig. 4). These changes are consistent with
358 the characteristics of activated microglia, as reported by Diz-Chaves et al, such as type IV microglia

359 (cells with large somas and retracted, thicker processes) and type V microglia (cells with amoeboid cell
360 bodies, numerous short processes, and intense Iba1 immunostaining) (Diz-Chaves et al., 2012).
361 Activated microglia in the CNS secrete proinflammatory cytokines and contribute to
362 neuroinflammation (Tsuda, Inoue, & Salter, 2005). Indeed, we found that *Pg* OMVs increased the levels
363 of pro-inflammatory cytokines such as IL-6, TNF- α , IL-8, and IL-1 β in a gingipain-dependent manner
364 in HMC3 cells (Fig. 5). Further experiments are needed to determine the expression levels of these
365 cytokines in gingipain-dependent brain tissue. Moreover, Tau protein was hyperphosphorylated in the
366 brains of *Pg* OMV-administered mice (Fig. 3). Both microglial activation and Tau
367 hyperphosphorylation have been shown to be related to the progression of AD (Perea et al., 2020). The
368 Tau protein is abnormally hyperphosphorylated and aggregates into neurofibrillary tangles (NFTs) in
369 the brains of patients with AD (J. Z. Wang, Xia, Grundke-Iqbal, & Iqbal, 2013). This
370 hyperphosphorylation of Tau is thought to impair the binding affinity of Tau to microtubules in neurons,
371 resulting in loss of neuronal integrity (Serrano-Pozo, Frosch, Masliah, & Hyman, 2011). Based on these
372 observations, it is possible that gingipains on *Pg* OMVs could induce neuroinflammation by activating
373 microglia; however, the direct effects of gingipains on microglia in the mouse brain were not elucidated
374 in the present study.

375

376 **5. Conclusion**

377 In summary, we show that *Pg* OMVs administered into the abdominal cavity were translocated to the
378 region around the lateral ventricle in the brain, as demonstrated by immunostaining for gingipains. *Pg*
379 OMVs were likely to reach around the lateral ventricle via the BCSFB because gingipains were also
380 detected in the choroid plexus and ventricular ependymal cells. In the *Pg* OMV-treated mouse brain,
381 both microglial activation and Tau hyperphosphorylation were observed. *Pg* OMVs also increased the
382 gene expression of proinflammatory cytokines in HMC-3 cells in a gingipain-dependent manner. Our
383 results suggest that *Pg* OMVs can reach the brain via the BCSFB and induce neuroinflammation by

384 activating microglia. These properties of *Pg* OMVs may provide a better understanding of the
385 implications of periodontal diseases in neurodegenerative conditions such as AD.

386

387 **Acknowledgements**

388 We thank the Support Center for Advanced Medical Sciences, Institute of Biomedical Sciences,
389 Tokushima University Graduate School for technical support.

390

391

392 **References**

- 393 Akiyama, H., Barger, S., Barnum, S., Bradt, B., Bauer, J., Cole, G. M., . . . Wyss-Coray, T.
394 (2000). Inflammation and Alzheimer's disease. *Neurobiology of Aging*, *21*(3), 383-421.
395 doi:10.1016/s0197-4580(00)00124-x
- 396 Diz-Chaves, Y., Pernía, O., Carrero, P., & Garcia-Segura, L. M. (2012). Prenatal stress causes
397 alterations in the morphology of microglia and the inflammatory response of the
398 hippocampus of adult female mice. *Journal of Neuroinflammation*, *9*, 71.
399 doi:10.1186/1742-2094-9-71
- 400 Dominy, S. S., Lynch, C., Ermini, F., Benedyk, M., Marczyk, A., Konradi, A., . . . Potempa, J.
401 (2019). Porphyromonas gingivalis in Alzheimer's disease brains: Evidence for disease
402 causation and treatment with small-molecule inhibitors. *Sci Adv*, *5*(1), eaau3333.
403 doi:10.1126/sciadv.aau3333
- 404 Eguchi, T., Sogawa, C., Okusha, Y., Uchibe, K., Iinuma, R., Ono, K., . . . Calderwood, S. K.
405 (2018). Organoids with cancer stem cell-like properties secrete exosomes and HSP90
406 in a 3D nanoenvironment. *PLoS One*, *13*(2), e0191109.
407 doi:10.1371/journal.pone.0191109
- 408 Farrugia, C., Stafford, G. P., & Murdoch, C. (2020). Porphyromonas gingivalis Outer
409 Membrane Vesicles Increase Vascular Permeability. *Journal of Dental Research*,
410 *99*(13), 1494-1501. doi:10.1177/0022034520943187
- 411 Farrugia, C., Stafford, G. P., Potempa, J., Wilkinson, R. N., Chen, Y., Murdoch, C., &
412 Widziolek, M. (2020). Mechanisms of vascular damage by systemic dissemination of
413 the oral pathogen Porphyromonas gingivalis. *FEBS Journal*. doi:10.1111/febs.15486
- 414 Furuta, N., Tsuda, K., Omori, H., Yoshimori, T., Yoshimura, F., & Amano, A. (2009).
415 Porphyromonas gingivalis outer membrane vesicles enter human epithelial cells via an
416 endocytic pathway and are sorted to lysosomal compartments. *Infection and Immunity*,
417 *77*(10), 4187-4196. doi:10.1128/iai.00009-09
- 418 Gabarrini, G., Grasso, S., van Winkelhoff, A. J., & van Dijk, J. M. (2020). Gingimaps: Protein
419 Localization in the Oral Pathogen Porphyromonas gingivalis. *Microbiology and
420 Molecular Biology Reviews*, *84*(1). doi:10.1128/mmmbr.00032-19
- 421 Genco, R. J., & Borgnakke, W. S. (2013). Risk factors for periodontal disease. *Periodontology*
422 *2000*, *62*(1), 59-94. doi:10.1111/j.1600-0757.2012.00457.x
- 423 Ghersi-Egea, J. F., & Strazielle, N. (2001). Brain drug delivery, drug metabolism, and
424 multidrug resistance at the choroid plexus. *Microscopy Research and Technique*, *52*(1),
425 83-88. doi:10.1002/1097-0029(20010101)52:1<83::Aid-jemt10>3.0.Co;2-n
- 426 Han, E. C., Choi, S. Y., Lee, Y., Park, J. W., Hong, S. H., & Lee, H. J. (2019). Extracellular
427 RNAs in periodontopathogenic outer membrane vesicles promote TNF- α production in

428 human macrophages and cross the blood-brain barrier in mice. *FASEB Journal*, 33(12),
429 13412-13422. doi:10.1096/fj.201901575R

430 Han, P., Bartold, P. M., Salomon, C., & Ivanovski, S. (2021). Salivary outer membrane vesicles
431 and DNA methylation of small extracellular vesicles as biomarkers for periodontal
432 status: A pilot study. *International Journal of Molecular Sciences*, 22(5), 2423.
433 doi:10.3390/ijms22052423

434 Ishida, N., Ishihara, Y., Ishida, K., Tada, H., Funaki-Kato, Y., Hagiwara, M., . . . Matsushita,
435 K. (2017). Periodontitis induced by bacterial infection exacerbates features of
436 Alzheimer's disease in transgenic mice. *NPJ Aging Mech Dis*, 3, 15.
437 doi:10.1038/s41514-017-0015-x

438 Kuehn, M. J., & Kesty, N. C. (2005). Bacterial outer membrane vesicles and the host-pathogen
439 interaction. *Genes and Development*, 19(22), 2645-2655. doi:10.1101/gad.1299905

440 Lippoldt, A., Jansson, A., Kniesel, U., Andbjør, B., Andersson, A., Wolburg, H., . . . Haller, H.
441 (2000). Phorbol ester induced changes in tight and adherens junctions in the choroid
442 plexus epithelium and in the ependyma. *Brain Research*, 854(1-2), 197-206.
443 doi:10.1016/s0006-8993(99)02355-0

444 Liu, Y., Wu, Z., Nakanishi, Y., Ni, J., Hayashi, Y., Takayama, F., . . . Nakanishi, H. (2017).
445 Infection of microglia with *Porphyromonas gingivalis* promotes cell migration and an
446 inflammatory response through the gingipain-mediated activation of protease-activated
447 receptor-2 in mice. *Scientific Reports*, 7(1), 11759. doi:10.1038/s41598-017-12173-1

448 Mandrekar-Colucci, S., & Landreth, G. E. (2010). Microglia and inflammation in Alzheimer's
449 disease. *CNS & Neurological Disorders Drug Targets*, 9(2), 156-167.
450 doi:10.2174/187152710791012071

451 Nara, P. L., Sindelar, D., Penn, M. S., Potempa, J., & Griffin, W. S. T. (2021). *Porphyromonas*
452 *gingivalis* Outer Membrane Vesicles as the Major Driver of and Explanation for
453 Neuropathogenesis, the Cholinergic Hypothesis, Iron Dyshomeostasis, and Salivary
454 Lactoferrin in Alzheimer's Disease. *Journal of Alzheimer's Disease*, 82(4), 1417-1450.
455 doi:10.3233/jad-210448

456 Nonaka, S., Kadowaki, T., & Nakanishi, H. (2022). Secreted gingipains from *Porphyromonas*
457 *gingivalis* increase permeability in human cerebral microvascular endothelial cells
458 through intracellular degradation of tight junction proteins. *Neurochemistry*
459 *International*, 154, 105282. doi:10.1016/j.neuint.2022.105282

460 Nonaka, S., & Nakanishi, H. (2020). Secreted gingipains from *Porphyromonas gingivalis*
461 induce microglia migration through endosomal signaling by protease-activated receptor
462 2. *Neurochemistry International*, 140, 104840. doi:10.1016/j.neuint.2020.104840

- 463 O'Brien-Simpson, N. M., Pathirana, R. D., Walker, G. D., & Reynolds, E. C. (2009).
464 Porphyromonas gingivalis RgpA-Kgp proteinase-adhesin complexes penetrate gingival
465 tissue and induce proinflammatory cytokines or apoptosis in a concentration-dependent
466 manner. *Infection and Immunity*, 77(3), 1246-1261. doi:10.1128/iai.01038-08
- 467 Oliver, C., González, C. A., Alvial, G., Flores, C. A., Rodríguez, E. M., & Bátiz, L. F. (2013).
468 Disruption of CDH2/N-cadherin-based adherens junctions leads to apoptosis of
469 ependymal cells and denudation of brain ventricular walls. *Journal of Neuropathology
470 and Experimental Neurology*, 72(9), 846-860. doi:10.1097/NEN.0b013e3182a2d5fe
- 471 Olsen, I. (2021). Porphyromonas gingivalis-Induced Neuroinflammation in Alzheimer's
472 Disease. *Frontiers in Neuroscience*, 15, 691016. doi:10.3389/fnins.2021.691016
- 473 Olsen, I., & Singhrao, S. K. (2020). Interaction between genetic factors, Porphyromonas
474 gingivalis and microglia to promote Alzheimer's disease. *Journal of Oral Microbiology*,
475 12(1), 1820834. doi:10.1080/20002297.2020.1820834
- 476 Ono, K., Eguchi, T., Sogawa, C., Calderwood, S. K., Futagawa, J., Kasai, T., . . . Kozaki, K. I.
477 (2018). HSP-enriched properties of extracellular vesicles involve survival of metastatic
478 oral cancer cells. *Journal of Cellular Biochemistry*, 119(9), 7350-7362.
479 doi:10.1002/jcb.27039
- 480 Perea, J. R., Bolós, M., & Avila, J. (2020). Microglia in Alzheimer's Disease in the Context of
481 Tau Pathology. *Biomolecules*, 10(10). doi:10.3390/biom10101439
- 482 Poole, S., Singhrao, S. K., Kesavalu, L., Curtis, M. A., & Crean, S. (2013). Determining the
483 presence of periodontopathic virulence factors in short-term postmortem Alzheimer's
484 disease brain tissue. *Journal of Alzheimer's Disease*, 36(4), 665-677. doi:10.3233/jad-
485 121918
- 486 Pritchard, A. B., Fabian, Z., Lawrence, C. L., Morton, G., Crean, S., & Alder, J. E. (2022). An
487 Investigation into the Effects of Outer Membrane Vesicles and Lipopolysaccharide of
488 Porphyromonas gingivalis on Blood-Brain Barrier Integrity, Permeability, and
489 Disruption of Scaffolding Proteins in a Human in vitro Model. *Journal of Alzheimer's
490 Disease*. doi:10.3233/jad-215054
- 491 Serrano-Pozo, A., Frosch, M. P., Masliah, E., & Hyman, B. T. (2011). Neuropathological
492 alterations in Alzheimer disease. *Cold Spring Harbor Perspectives in Medicine*, 1(1),
493 a006189. doi:10.1101/cshperspect.a006189
- 494 Seyama, M., Yoshida, K., Yoshida, K., Fujiwara, N., Ono, K., Eguchi, T., . . . Ozaki, K. (2020).
495 Outer membrane vesicles of Porphyromonas gingivalis attenuate insulin sensitivity by
496 delivering gingipains to the liver. *Biochim Biophys Acta Mol Basis Dis*, 1866(6),
497 165731. doi:10.1016/j.bbadis.2020.165731

- 498 Singhrao, S. K., & Olsen, I. (2018). Are Porphyromonas gingivalis Outer Membrane Vesicles
499 Microbullets for Sporadic Alzheimer's Disease Manifestation? *J Alzheimers Dis Rep*,
500 2(1), 219-228. doi:10.3233/adr-180080
- 501 Takii, R., Kadowaki, T., Baba, A., Tsukuba, T., & Yamamoto, K. (2005). A functional
502 virulence complex composed of gingipains, adhesins, and lipopolysaccharide shows
503 high affinity to host cells and matrix proteins and escapes recognition by host immune
504 systems. *Infection and Immunity*, 73(2), 883-893. doi:10.1128/iai.73.2.883-893.2005
- 505 Tsuda, M., Inoue, K., & Salter, M. W. (2005). Neuropathic pain and spinal microglia: a big
506 problem from molecules in "small" glia. *Trends in Neurosciences*, 28(2), 101-107.
507 doi:10.1016/j.tins.2004.12.002
- 508 Wang, J. Z., Xia, Y. Y., Grundke-Iqbal, I., & Iqbal, K. (2013). Abnormal hyperphosphorylation
509 of tau: sites, regulation, and molecular mechanism of neurofibrillary degeneration.
510 *Journal of Alzheimer's Disease*, 33 Suppl 1, S123-139. doi:10.3233/jad-2012-129031
- 511 Wang, W. Y., Tan, M. S., Yu, J. T., & Tan, L. (2015). Role of pro-inflammatory cytokines
512 released from microglia in Alzheimer's disease. *Ann Transl Med*, 3(10), 136.
513 doi:10.3978/j.issn.2305-5839.2015.03.49
- 514 Yoshiyama, Y., Higuchi, M., Zhang, B., Huang, S. M., Iwata, N., Saido, T. C., . . . Lee, V. M.
515 (2007). Synapse loss and microglial activation precede tangles in a P301S tauopathy
516 mouse model. *Neuron*, 53(3), 337-351. doi:10.1016/j.neuron.2007.01.010
517
- 518

519 **Figure Legends**

520 **Figure 1: Gingipains were detected around the cerebral ventricle in *Pg* OMV-administered mice**

521 The mice were administered PBS (a, b) or *Pg* OMVs (c-f) for 12 weeks, and the brain tissue sections
522 were stained with an anti-gingipain antibody (a-e) or normal rabbit IgG (f). The regions of the red boxes
523 (a, c) are shown at higher magnification (b, d). A higher magnification of the region of the black box in
524 (d) is shown in (e) and (f). Open arrowheads indicate specific anti-gingipain antibody staining (d and
525 e). Scale bars indicate 200 μm (a, c), 100 μm (b, d), or 20 μm (e, f). Abbreviations: Hp, hippocampus;
526 V, cerebral ventricle; Cp, choroid plexus.

527

528 **Figure 2: Gingipains were detected in the choroid plexus and ventricular ependymal cells of *Pg***
529 **OMV-administered mice**

530 Immunohistochemical detection of gingipains in the choroid plexus (b, e, f) and ventricular ependymal
531 cells (c, g, h) of brain tissues from mice administered PBS (a–c) or *Pg* OMVs (d–h) for 12 weeks. The
532 regions indicated by red boxes in (a) and (d) are shown at higher magnifications in (b, d) and (e, g),
533 respectively.

534 Specific gingipain staining in the perinuclear region of the choroid plexus epithelial cells (e, closed
535 arrowheads), blood vasculature within the choroid plexus (e, arrows), and extracellular spaces (e,
536 opened arrowheads). Detection of gingipains in the perinuclear regions of ependymal cells (g, closed
537 arrowheads) and extracellular spaces (g, opened arrowheads). The scale bars represent 200 μm (a, d),
538 or 20 μm (b, c, e, f, g, h). Hp, hippocampus; V, cerebral ventricle; Cp, choroid plexus.

539

540 **Figure 3: Tau and phosphorylated-Tau protein levels increased in the brains from *Pg* OMV-**
541 **administered mice**

542 Brains were excised from the mice administered PBS or *Pg* OMVs for 12 weeks. (A) Lysates of the
543 brain tissue were analyzed by western blotting using anti-phospho-Tau (p-Tau), anti-Tau, and GAPDH.
544 (B) Densitometry of Tau and phosphorylated-Tau (p-Tau) was normalized to that of GAPDH. The ratios

545 of Tau/GAPDH and p-Tau/GAPDH in each group are presented for mice treated with PBS (n = 4) or
546 *Pg* OMV (n = 4) and analyzed by the Student's *t*-test. Values are shown as the fold change in expression
547 levels in the PBS group. * $p < 0.05$, ** $p < 0.01$ as compared with mice treated with PBS.

548

549 **Figure 4: Microglia were activated in the brains from *Pg* OMVs-administered mice**

550 The mice were administered PBS (a-c) or *Pg* OMVs (d-f) for 12 weeks, and the brain tissue sections
551 were stained with anti-Iba1 antibody. Iba1 staining in the region around the cerebral ventricle (A) and
552 hippocampus (B). The region of the red boxes (a, d) is shown at a higher magnification (b, e). Higher
553 magnifications of b and e are shown in c and f, respectively. Open arrowheads indicate activated
554 microglia. Scale bars indicate 200 μm (a, d), 50 μm (b, e), and 20 μm (c, f). The scale bars indicate
555 20 μm . "V" means cerebral ventricle.

556

557 **Figure 5: *Pg* OMVs increased the expression of proinflammatory cytokine genes in a gingipain-
558 dependent manner in HMC3 cells**

559 HMC3 cells were treated with 500 ng/mL *Pg* OMVs for 3 h. The mRNA expression in HMC3 cells
560 treated with PBS (n = 4), *Pg* OMVs (WT) (n = 4), or *Pg* OMVs (K136) (n = 4) was analyzed using real-
561 time PCR. Values are shown as the fold change in expression levels in the PBS group. Student's *t*-test
562 was used for statistical analysis. * $p < 0.05$, ** $p < 0.01$ compared each group.

563

Figure 1. Gingipains were detected around the cerebral ventricle in *Pg* OMV-administered mice

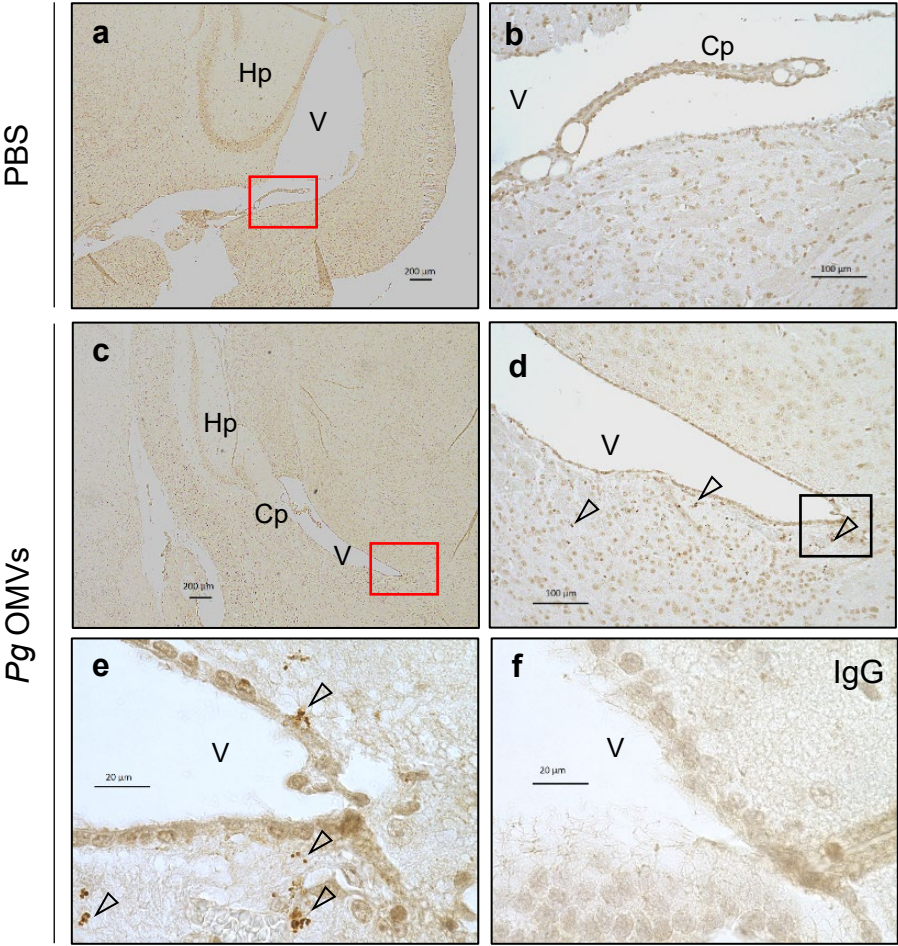


Figure 2. Gingipains were detected in the choroid plexus and ventricular ependymal cells of *Pg* OMV-administered mice

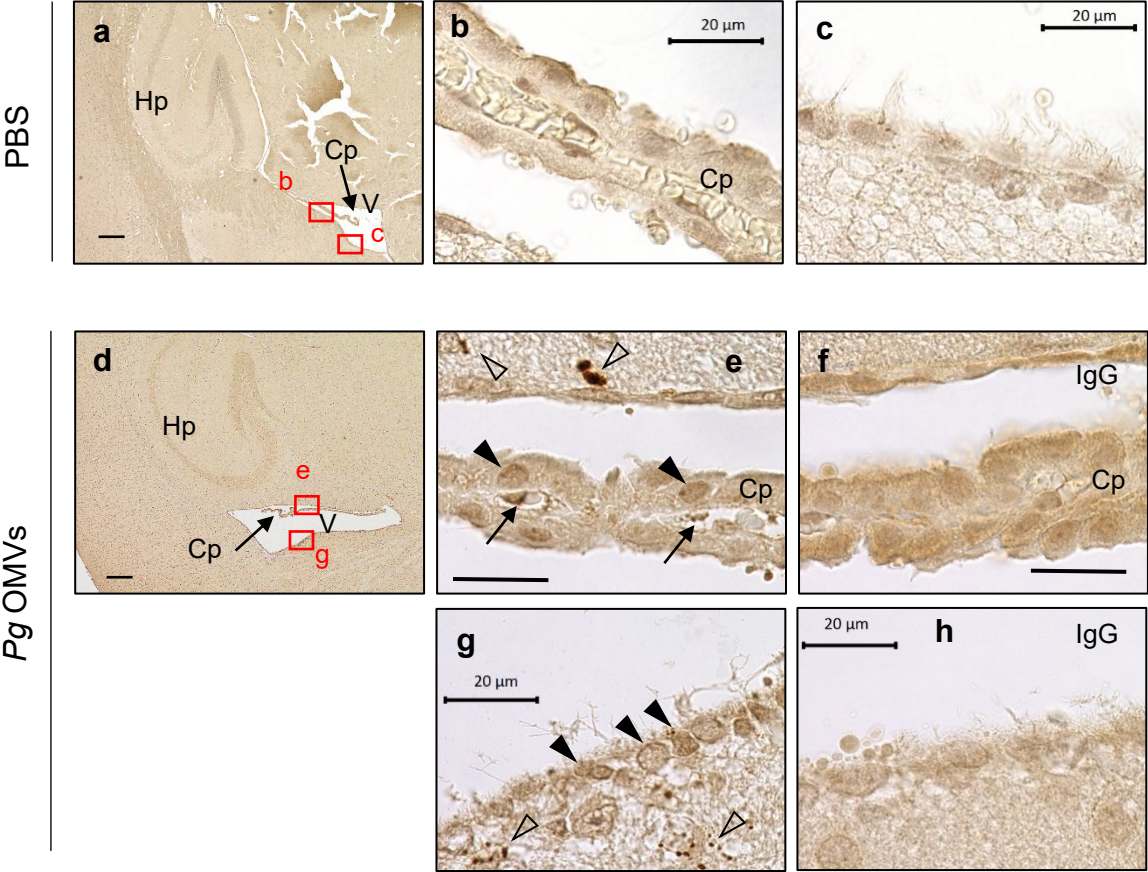
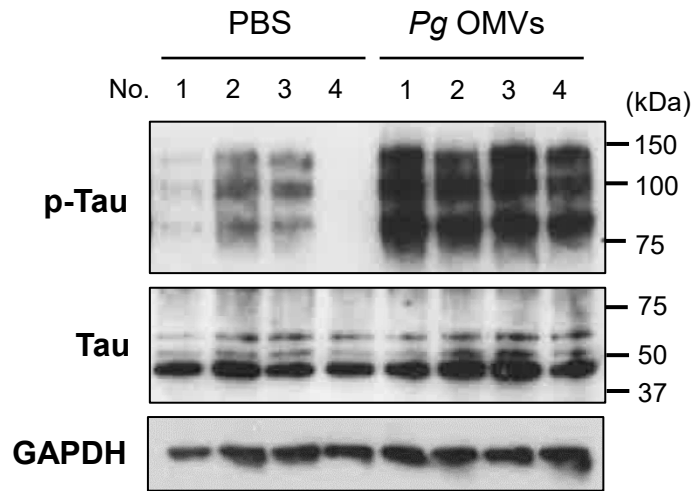


Figure 3. Tau and phosphorylated-Tau protein levels increased in the brains from *Pg* OMV-administered mice

A



B

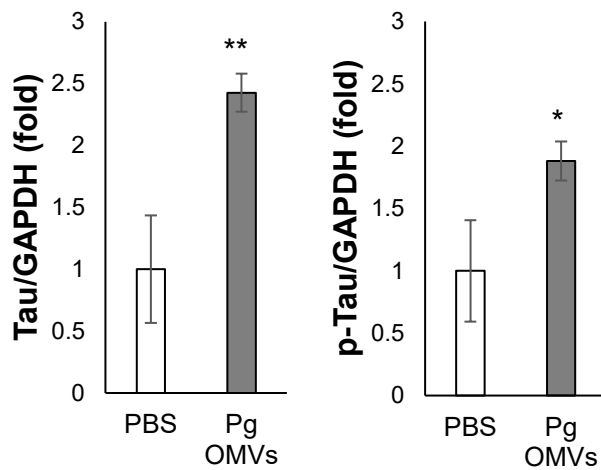


Figure 4. Microglia were activated in the brains from *Pg* OMVs-administered mice

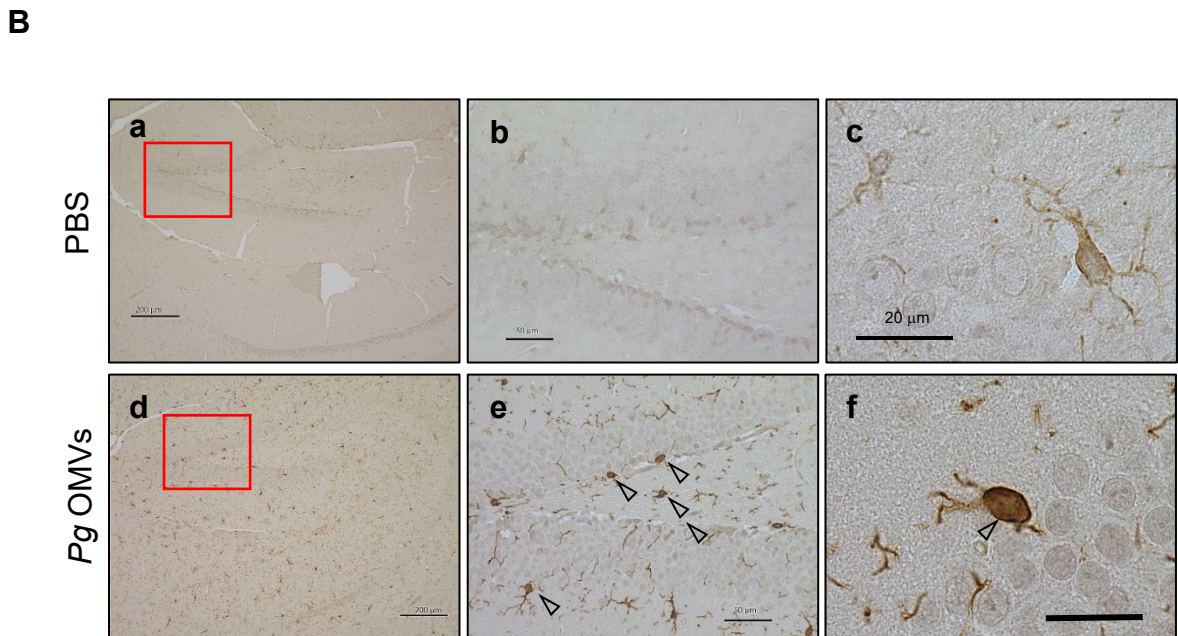
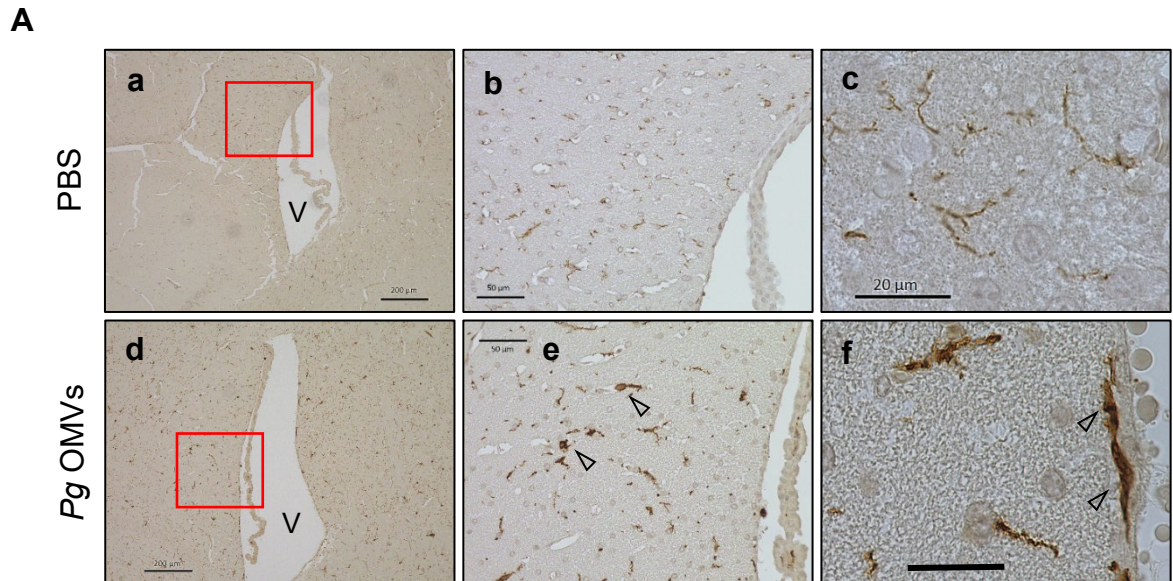


Figure 5. *Pg* OMVs increased the expression of proinflammatory cytokine genes in a gingipain-dependent manner in HMC3 cells

